metals

MDPI

Article

Hydrostatic Equation of State of *bcc* Bi by Directly Solving the Partition Function

Yue-Yue Tian [1,2], Bo-Yuan Ning [3], Hui-Fen Zhang [1,2,4,*] and Xi-Jing Ning [1,2,*]

[1] Institute of Modern Physics, Fudan University, Shanghai 200433, China; 21110200031@m.fudan.edu.cn
[2] Applied Ion Beam Physics Laboratory, Fudan University, Shanghai 200433, China
[3] Shanghai Institute of Applied Physics, Chinese Academy of Sciences, Shanghai 201800, China; ningboyuan@sinap.ac.cn
[4] Hongzhiwei Technology (Shanghai) Co., Ltd., Shanghai 201206, China
* Correspondence: huifen_zhang@fudan.edu.cn (H.-F.Z.); xjning@fudan.edu.cn (X.-J.N.)

Abstract: Body-centered cubic bismuth (Bi) is considered to be an enticing pressure marker, and, therefore, it is highly desirable to command its accurate equation of state (EOS). However, significant discrepancies are noted among the previous experimental EOSs. In the present work, an EOS of up to 300 GPa is theoretically obtained by solving the partition function via a direct integral approach (DIA). The calculated results nearly reproduce the hydrostatic experimental measurements below 75 GPa, and the deviations from the measurements gradually become larger with increasing pressure. Based on the ensemble theory of equilibrium state, the DIA works with high precision particularly in high-pressure conditions, so the hydrostatic EOS presented in this work is expected to be a reliable pressure standard.

Keywords: equation of state; bismuth; partition function; ensemble theory of equilibrium state; direct integral approach; hydrostatic condition

Citation: Tian, Y.-Y.; Ning, B.-Y.; Zhang, H.-F.; Ning, X.-J. Hydrostatic Equation of State of *bcc* Bi by Directly Solving the Partition Function. *Metals* **2024**, *14*, 601. https://doi.org/10.3390/met14050601

Academic Editor: Alain Pasturel

Received: 4 April 2024
Revised: 11 May 2024
Accepted: 17 May 2024
Published: 20 May 2024

1. Introduction

Metal bismuth (Bi), crystalizing in a rhombohedral structure at ambient conditions, undergoes a series of pressure-induced transitions in the sequence of the rhombohedral phase → monoclinic phase → body-centered tetragonal phase → body-centered cubic (*bcc*) phase [1–7] at 2.55, 2.7, and 7.7 GPa, respectively. All these room-temperature transition points are clear and have been widely used for pressure calibration. Especially, *bcc* Bi is enticing as an internal pressure standard because (i) it is stable over a wide pressure range (7.7–299 GPa) [7–10]; (ii) it has the highest atomic number of any non-radioactive element, bringing about strong X-ray diffraction signals; and (iii) its bulk modulus (35.2–54.7 GPa [10,11]) is much smaller than that of most other pressure standards (such as Ta 194 GPa [12], Au 167 GPa [13], and W 310 GPa [14]), giving rise to larger volume changes under the same pressure. So, using *bcc* Bi for pressure calibration is expected to improve the pressure measurements in high-pressure research. However, the high-pressure (>50 GPa) experimental investigations on the equation of state (EOS) of *bcc* Bi are very limited, and only four [8–11] experiments have been reported in the last two decades. What is more, among these measured EOSs, significant discrepancies are noted, particularly in the high-pressure range. We think two aspects should mainly be considered regarding this disparity.

First, the evaluations of pressure in static research depend strongly on a secondary pressure scale, and the determined values may be quite different based on the different scales in a single experiment. For example, Akahama et al. [10] pointed out that, if the Au pressure scale promoted by Jamieson et al. [15] were used to calibrate the pressure in their experiment for the EOS of Bi, the determined pressures above 30 GPa would be observably smaller than those obtained via the Pt gauge of Holmes et al. [16], and,

with increasing compression, the difference consistently rises high, up to ~20 GPa around 150 GPa. Campbell et al. [9] conducted quasi-hydrostatic high-pressure investigations for Bi and showed that the EOS over 100 GPa presents an apparent difference between the results of two neon scales, and Dewaele et al. [17] found, while calibrating the pressure, that the discrepancy reaches ~10 GPa around 250 GPa. Obviously, the accuracy of the pressure values determined in static experiments relies intimately on the precision of the adopted calibrants. In fact, the currently available pressure standards originated from fitting or further extrapolating limited measurements with empirical equations, such as Vinet [18,19], third-order Birch–Murnaghan [20,21], AP2 [22,23], and so on. As the empirical functions are usually built on a limited physics basis and the evaluated pressures are always disparate using different equations or even using the same equation [24,25], the predicted results may be significantly diverse with different input data. So, most pressure scales at present are not unified, and the discrepancies generally present more and more with increasing pressure.

To obtain quasi-hydrostatic pressures, it is typically required to load the samples with a pressure-transmitting medium (PTM) in diamond anvil cell (DAC) experiments. Whereas, Bi itself with a low yield/shear strength [26] is regarded as a good PTM, and, in some of the previous static high-pressure studies for the EOS of Bi, no other PTM was used, counting on the Bi itself to redistribute the anisotropic stress. It was revealed that, with no additional PTM, the uniaxial stress component in the compressed sample Bi was relatively small [8–11], but non-negligible deviatoric stresses were found in the concurrently compressed pressure markers, which may arouse significant errors for the determination of pressure. For example, a very recent experiment conducted by Storm et al. [8] without any other PTM showed that a correction for the pressure (279 GPa) evaluated from the used Au gauge due to a non-hydrostatic effect reached 39 GPa, meaning that a relative indeterminacy of 13% at ~300 GPa was present in their reported Bi EOS. It should be pointed out that the non-hydrostatic effect on different pressure scales is different, hinging on their inherent incompressibility. For example, the pressure corrections due to the gradient stress of the Pt calibrant used in the experiments in Ref. [10] and the Cu scale used in Ref. [8] were significantly smaller than for the Au in Ref. [8]. So, the second factor accounting for the inconsistency regarding the previous experimental EOSs of *bcc* Bi is the different degrees of the non-hydrostatic effect on the pressure markers in terms of if there is an additional PTM and what pressure scales were used in the experiments.

As mentioned above, the high-pressure experimental EOSs of *bcc* Bi are controversial at present, and it is necessary to confront this issue in a theoretical way. In fact, the ensemble theory offers a promising avenue for accurate EOSs of condensed matter as long as the partition function (PF) or free energy (FE) is calculated precisely. It is known that exactly solving the PF involving a 3*N*-fold configurational integral far exceeds the capability of the current computer technologies, so the EOS of *bcc* Bi has never been calculated by directly solving the PF at the level of the first principles calculating the interatomic energies. Recently, a direct integral approach (DIA) to the PF with ultrahigh precision and efficiency was established by Ning et al. [27] and has been successfully used to calculate the EOSs of solid copper [27], iridium [28], argon [29], and 2-D materials [30], and to reproduce the phase transitions of crystal vanadium [31], zirconium [32], and aluminum [33]. In particular, a very recent work on the high-temperature and simultaneously high-pressure EOS of tungsten [34] showed that, compared with the available static compression experiments, all the deviations in the calculated results by the DIA were within or comparable to the uncertainty of the experiments. In this work, a DIA is applied to calculate the PF of crystal *bcc* Bi as well as the hydrostatic room-temperature EOS up to 300 GPa. The details for the implementation of the DIA are elaborated on in Section 2. Careful comparisons and a discussion of the calculated results with the available experiments are presented, respectively, in Sections 3 and 4, and the final section is the conclusion.

2. Calculation Method

For a crystal containing N atoms of atomic mass m confined within volume V at temperature T, the atoms are regarded as N point particles with cartesian coordinate $\boldsymbol{q}^N = \{\boldsymbol{q}_1, \boldsymbol{q}_2, \cdots \boldsymbol{q}_N\}$, and the total energy, $U(\boldsymbol{q}^N)$, as the function of $\boldsymbol{q}^N$ can be computed by quantum mechanics. With the knowledge of $U(\boldsymbol{q}^N)$, the PF of the system reads

$$Z = \frac{1}{N!}\left(\frac{2\pi m}{\beta h^2}\right)^{\frac{3}{2}N} \int d\boldsymbol{q}^N e^{-\beta U(\boldsymbol{q}^N)} = \frac{1}{N!}\left(\frac{2\pi m}{\beta h^2}\right)^{\frac{3}{2}N} \mathcal{Q}, \tag{1}$$

where h is the Planck constant and $\beta = 1/k_B T$ with k_B the Boltzmann constant. If the configurational integral $\mathcal{Q} = \int d\boldsymbol{q}^N e^{-\beta U(\boldsymbol{q}^N)}$ is solved, the pressure (P),

$$P = \frac{1}{\beta}\frac{\partial ln Z}{\partial V}, \tag{2}$$

Helmholtz FE (F),

$$F = -\frac{1}{\beta} ln Z, \tag{3}$$

and any other thermodynamic quantities can be gained.

For a crystal with all the N atoms placed in their lattice sites $\boldsymbol{Q}^N = \{\boldsymbol{Q}_1, \boldsymbol{Q}_2, \cdots, \boldsymbol{Q}_N\}$ and with the total potential energy $U_0\left(\boldsymbol{Q}^N\right)$, we first introduce a transformation [27],

$$\boldsymbol{q}'^N = \boldsymbol{q}^N - \boldsymbol{Q}^N,\ U'\left(\boldsymbol{q}'^N\right) = U\left(\boldsymbol{q}^N\right) - U_0\left(\boldsymbol{Q}^N\right), \tag{4}$$

where $\boldsymbol{q}'^N$ represents the displacements of atoms away from their equilibrium positions. Then, the $\mathcal{Q}$ is expressed as

$$\mathcal{Q} = e^{-\beta U_0} \int d\boldsymbol{q}'^N e^{-\beta U'(\boldsymbol{q}'^N)}. \tag{5}$$

According to DIA [27], the above $3N$-fold integral could be approximated as

$$\mathcal{Q} = e^{-\beta U_0} \prod_{i=1}^{N} (\mathcal{L}_{ix}\mathcal{L}_{iy}\mathcal{L}_{iz}) \tag{6}$$

with the effective length

$$\begin{aligned} \mathcal{L}_{ix} &= \int e^{-\beta U'(0\cdots q'_{ix}\ \cdots 0)} dq'_{ix}, \\ \mathcal{L}_{iy} &= \int e^{-\beta U'(0\cdots q'_{iy}\ \cdots 0)} dq'_{iy} \end{aligned} \tag{7}$$

and

$$\mathcal{L}_{iz} = \int e^{-\beta U'(0\cdots q'_{iz}\cdots 0)} dq'_{iz},$$

where q'_{ix} (q'_{iy} or q'_{iz}) is the x (y or z) coordinate of the ith atom moving away off its ideal lattice site along with the other two degrees of freedom of the atom and all the degrees of freedom of the other atoms fixed.

For crystal *bcc* Bi, all the atoms are equivalent, and, therefore, the $\mathcal{Q}$ in Equation (6) turns into

$$\mathcal{Q} = e^{-\beta U_0} \left(\mathcal{L}_x \mathcal{L}_y \mathcal{L}_z\right)^N. \tag{8}$$

Clearly, if orientations [100], [010], and [001] are selected as the three axes of a Cartesian system, $\mathcal{L}_x$, $\mathcal{L}_y$, and $\mathcal{L}_z$ are equal, and the $\mathcal{Q}$ could be calculated by

$$\mathcal{Q} = e^{-\beta U_0} (\mathcal{L}_x)^{3N}. \tag{9}$$

To implement the calculations, a 3 × 3 × 3 supercell containing 54 atoms arranged in a *bcc* structure was constructed (Figure 1a). First, the system was fully relaxed to make the stresses on all the atoms isotropic, and the optimized lattice constant is a_0 (Figure 1a) and the total energy is U_0. Then, an arbitrary atom (in the red circle) was moved away along [100] direction step by step with an interval of 0.02 Å. At each step, the total energy of the system $U(x)$ was calculated with the lattice and all the atoms frozen. The completed $U'(x') = U(x) - U_0$ (Figure 1b) was smoothed by the cubic spline interpolation algorithm [35] to compute $\mathcal{L}_x$ via Equation (7) with the integral step of 10^{-5} Å. Finally, the corresponding PF was obtained based on Equations (1) and (9). Changing the volume of the supercell by enlarging or shrinking the lattice constant a_0 and repeating the above process without optimizing the supercell, a series of U_0 and $U'(x')$ as a function of the volume can be obtained (Figure 1b). Accordingly, room-temperature PF vs. V, and, further, the corresponding P–V relationship, were achieved by Equation (2).

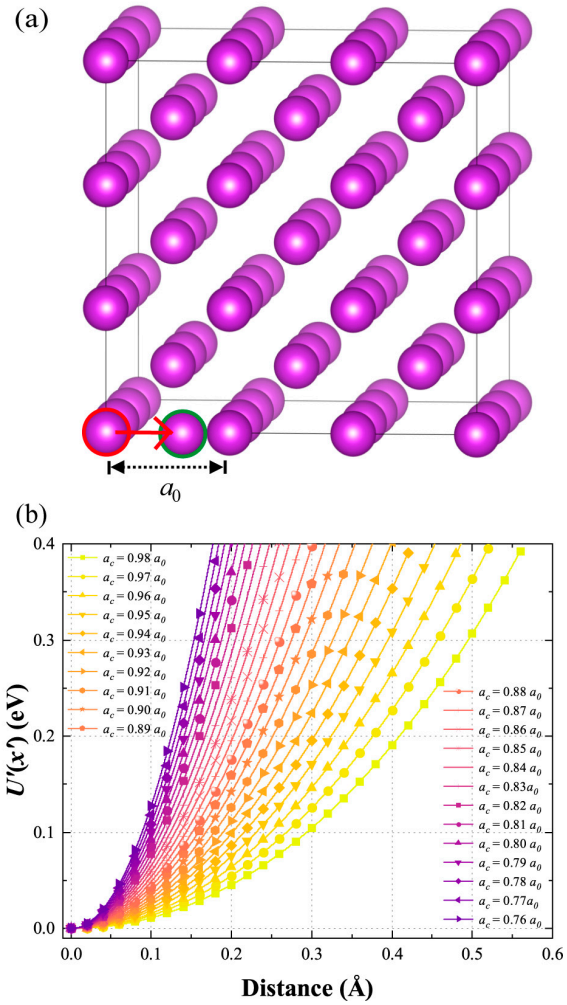

Figure 1. (color online) A 3 × 3 × 3 supercell of *bcc* Bi with optimized lattice constant a_0, in which an arbitrary atom in the red circle is moved along the [100] direction (red arrow) step by step until its final position labeled in the green circle to obtain $U'(x')$ (**a**); dependence of $U'(x')$ on the distance of the moved atom away from its equilibrium position x' under a series of volumes with lattice constant a_c changed from 0.76 a_0 to 0.98 a_0 (**b**).

All the above calculations were completed by density functional theory (DFT) and performed in the Vienna Ab initio Simulation Package (VASP) [36,37]. The projector augmented wave (PAW) pseudopotential [38,39] with $6s^2 6p^3$ as the valence states was adopted for describing the electron–ion interactions, and the generalized gradient approximation

(GGA) parametrized by Perdew–Burke–Ernzerhof (PBE) [40] was employed to consider the exchange-correlation functional of the electrons since PBE [40] has been frequently used in Bi-based structures and phases [41–44]. In the first step of optimizing the structure, the forces that acted on every atom were less than 0.02 eV/Å when the relaxation was converged. For the calculations of the total energies, electron self-consistent tolerance was 2×10^{-6} eV, which is fine enough regarding the integral in Equation (7). A Γ-centered $11 \times 11 \times 11$ uniform *k*-mesh was set to sample the Brillouin zone by the Monkhorst–Pack scheme, and the tetrahedron method with Blöchl corrections was adopted to determine the electron orbital partial occupancy with the plane-wave cut-off energy of 350 eV. Convergence tests of all these parameters were performed for the structure with the smallest volume ($a_c = 0.76\ a_0$) taking the fluctuation of the total energy less than 10^{-3} eV/atom. Unquestionably, the precision of the total energy calculations for the larger volume structures would not degrade under the same parameters.

3. Results

The calculated data of the isothermal EOS of *bcc* Bi at 300 K are listed in Table 1. The *P*–*V* curve as well as four sets of experimental measurements [8–11] and the theoretical result (up to 220 GPa) by Mukherjee et al. [45] under the Debye model (DM) are displayed in Figure 2. It is noted that the theoretically calculated volumes at given pressures are consistently larger than the experimental measurements (Figure 2a). Taking the volume at 7.7 GPa as an example, the values calculated by the DIA and DM are 28.58 and 27.86 Å^3/atom, respectively, and the experimentally measured values are 27.44–27.63 Å^3/atom [8–10]. To avoid this system offset and make specific comparisons between the theoretical calculations and experimental results, relative volume vs. pressure was usually used in previous studies [46–48] and is also adopted in the present work, which should be feasible considering that the curvature of the *P*–*V* curve calculated by the DIA is very similar to that of the experimental dataset. Since *bcc* Bi was recognized to emerge at 7.7 GPa [7,8,11,45], the relative volume $V/V_{7.7}$ with $V_{7.7}$ the atomic volume at 7.7 GPa is used to express the EOS (Figure 2b), and all the discussions in this work start from 7.7 GPa. Under the same value of $V/V_{7.7}$, the deviations in the calculated pressure from the DIA (P_{DIA}) or DM (P_{DM}) with the experimental measurements (P_{Exp}) are exhibited in Figure 3.

Table 1. Relative volume ($V/V_{7.7}$) as a function of pressure (in GPa). $V_{7.7}$ is the calculated atomic volume (28.58 Å^3/atom) of *bcc* Bi under 7.7 GPa at 300 K.

P	*V*
7.7	1.0000
10	0.9728
20	0.8891
30	0.8311
40	0.7890
50	0.7545
60	0.7265
70	0.7026
80	0.6819
90	0.6637
100	0.6474
110	0.6328
120	0.6197
130	0.6077
140	0.5965
150	0.5862
160	0.5766
170	0.5677
180	0.5593
190	0.5515

Table 1. *Cont.*

P	*V*
200	0.5441
210	0.5370
220	0.5303
230	0.5240
240	0.5180
250	0.5122
260	0.5068
270	0.5015
280	0.4965
290	0.4916
300	0.4870

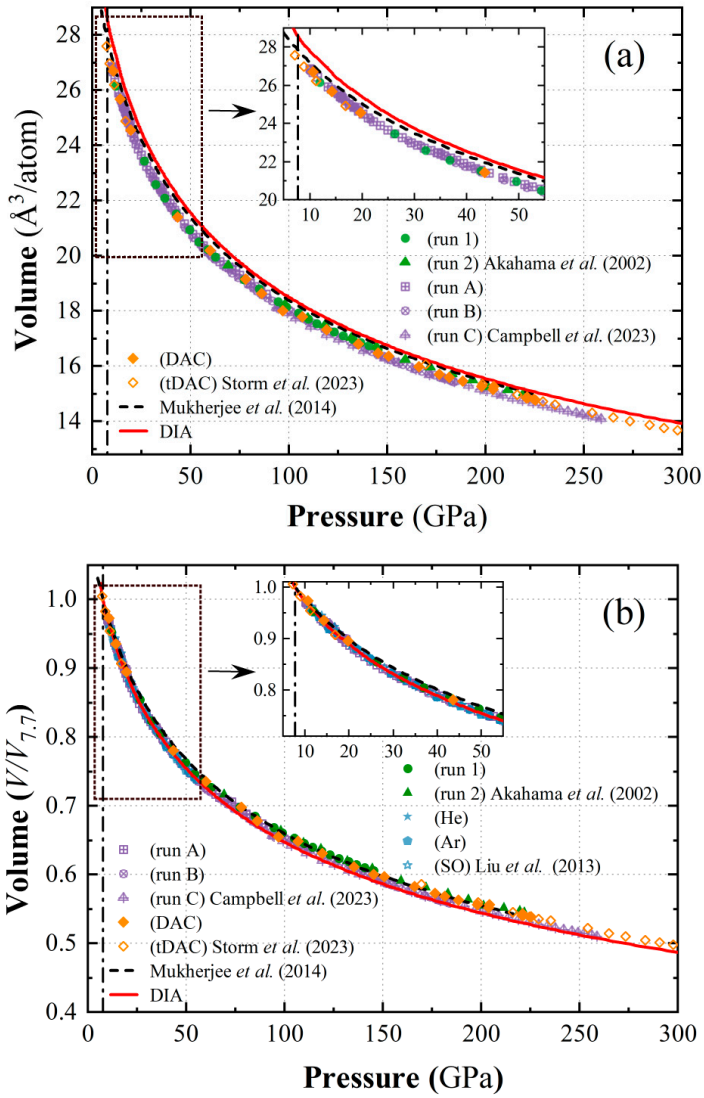

Figure 2. (color online) Absolute volume (V) (**a**) and relative volume ($V/V_{7.7}$) (**b**) vs. pressure of *bcc* Bi with $V_{7.7}$ the volume under 7.7 GPa at 300 K. The red solid and black dashed lines are the calculated curves by DIA and the Debye model (adapted from Ref. [45]), respectively. The measurements in two experimental runs performed by Akahama et al. (adapted from [10]) are respectively represented by the green dots (run 1) and triangles (run 2). Campbell et al. (adapted from Ref. [9]) provided three sets of compressed data denoted by the purple squares (run A), circles (run B), and triangles

(run C). The orange solid and open diamonds represent the two sets of experimental measurements conducted in a conventional and toroidal DACs (tDAC) by Storm et al. (adapted from Ref. [8]). Liu et al. (adapted from Ref. [11]) investigated the EOS of Bi using He, Ar, and silicone oil (SO) as the PTM, and the corresponding measurements are shown by the blue solid stars (He), pentagons (Ar), and open stars (SO), respectively, which are not exhibited in (**a**) because absolute volumes of Bi were not presented in their work. Since *bcc* Bi was recognized to emerge at 7.7 GPa (marked by the vertical dash dotted line in (**a**,**b**), all the discussions in the context start from 7.7 GPa.

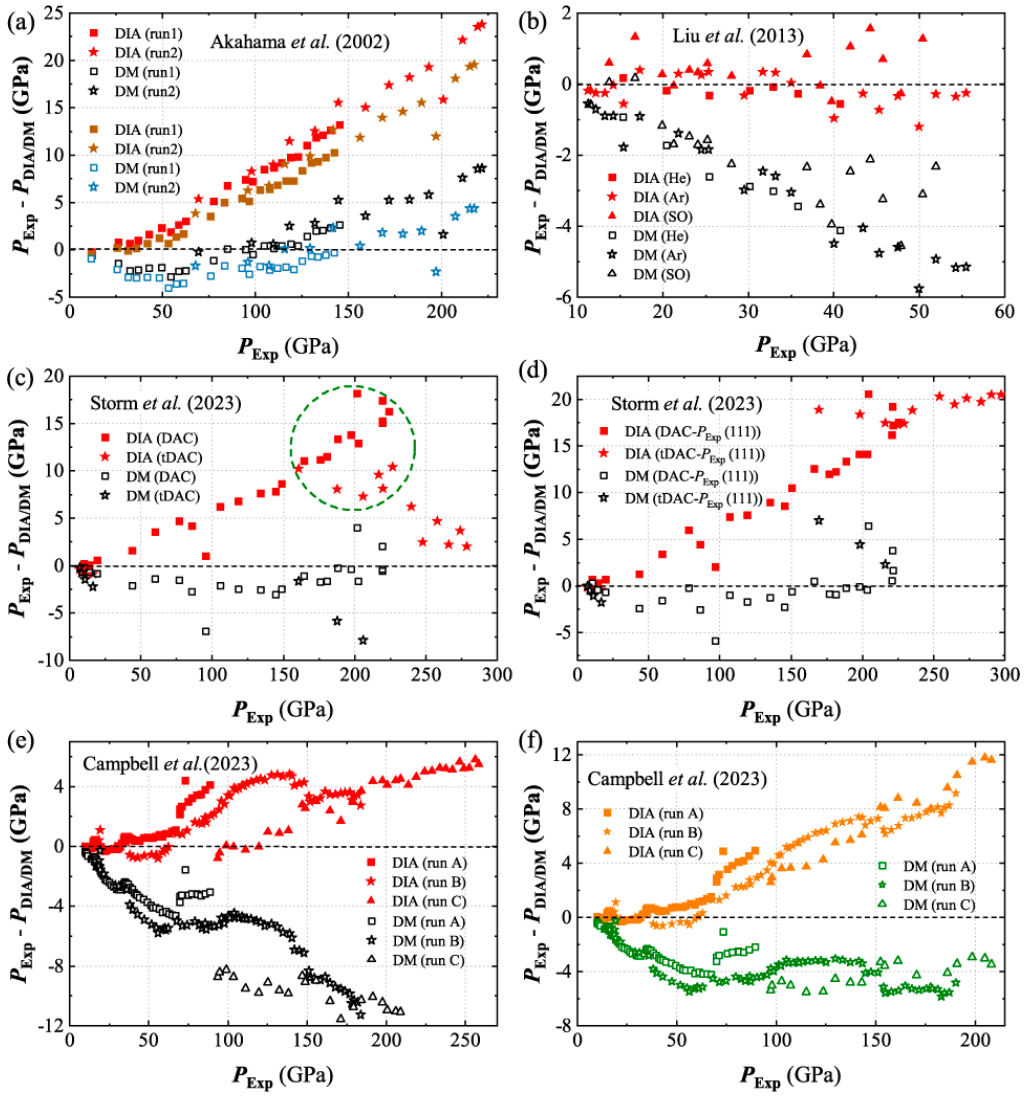

Figure 3. Under the same value of $V/V_{7.7}$, differences between the calculated pressure by DIA (P_{DIA}) or the Debye model (P_{DM}) (adapted from Ref. [45]) with the in situ experimental measurements (P_{Exp}) adapted from Refs. [8–11] are displayed as the red or black symbols in (**a**–**c**,**e**), respectively. After the pressures in Ref. [10] are re-evaluated by the latest Pt scale proposed by Fratanduono et al. (adapted from Ref. [49]), the deviations between P_{DIA} or P_{DM} with the re-calibrated pressures are respectively displayed by the brown or blue symbols in (**a**). If the X-ray diffraction peaks of only the (111) lattice plane of the used Cu and Au pressure markers are selected to determine the pressures (labeled by P_{Exp} (111)) in Ref. [8], the deviations in P_{DIA} or P_{DM} with P_{Exp} (111) from Ref. [8] are presented in (**d**). For the pressures in the first two experimental runs (run A and run B) and the third one (run C) of Ref. [9], recalibrating was performed with the latest Cu pressure gauge of Fratanduono et al. (adapted from Ref. [50]) and the neon EOS of Dewaele et al. (adapted from Ref. [17]), respectively, and the deviations in P_{DIA} or P_{DM} with the re-estimated pressures are represented by the corresponding orange and green symbols in (**f**).

Akahama et al. [10] carried out two sets of experiments in conventional DACs and measured the unit cell volumes of Bi up to 145 and 222 GPa, respectively. Compared with the P_{Exp}, the P_{DIA} manifests consistently smaller in the whole pressure range, and the difference, $P_{Exp} - P_{DIA}$, increases gradually with increasing pressure up to 23.8 GPa (red symbols in Figure 3a) at the highest compression, corresponding to a relative error ($(P_{Exp} - P_{DIA})/P_{Exp}$) of ~11%. On the other hand, the P_{DM} presents much closer to the P_{Exp} in the high-pressure scope (>70 GPa) (black symbols in Figure 3a). In fact, the Pt pressure scale of Holmes et al. [16] used in this experiment has been revealed to overestimate pressures [51]. As the authors of Ref. [10] pointed out, if the Au calibration of Jamieson et al. [15] were adopted to evaluate the pressures, the values would be lower than those estimated from Holmes' Pt, and the highest pressure in their first experimental run would be 128.9 GPa (instead of 145 GPa), which is less than the P_{DIA} by only ~3 GPa while smaller than the P_{DM} by ~13 GPa. Considering that systematic errors arising from the selected pressure scale may exist in the Bi EOS of Akahama et al., we re-calibrate the pressures in Ref. [10] with the latest Pt standard established by Fratanduono et al. [49]. As shown by the brown symbols in Figure 3a, the re-calibrated pressures are indeed smaller than those evaluated from Holmes' Pt, and the largest difference between the P_{DIA} and the re-determined pressure reduces to 19.5 GPa, corresponding to a relative error of 9%. Comparatively, the average difference between the P_{DM} and the re-estimated pressure is much smaller, with an average relative deviation ($|P_{Exp} - P_{DM}|/P_{Exp}$) of only 2.7% (blue symbols in Figure 3a).

Liu et al. [11] inspected the influence of different PTMs on the EOS of Bi using a DAC and found that the measured results up to 55 GPa were consistent with each other when He, Ar, and silicone oil (SO) PTM were used. As shown in Figure 3b, the three sets of extremely self-consistent experimental data under different PTMs are nearly reproduced by the DIA, and the differences between the P_{DIA} and P_{Exp} fluctuate around zero in the experimental condition, with an average $|P_{Exp} - P_{DIA}|$ of only 0.48 GPa, which is entirely within the uncertainty of the P_{Exp} arising from the used ruby pressure scale in the experiments. On the other hand, the P_{DM} deviates from the P_{Exp} more and more with increasing pressure, and the relative error ($|P_{Exp} - P_{DM}|/P_{Exp}$) reaches ~9.3% at the highest compression.

Storm et al. [8] conducted diffraction studies of Bi up to 298 GPa using both conventional and toroidal DACs (tDAC) to investigate the EOS without an additional PTM. As the red squares in Figure 3c showed, the difference between the P_{DIA} and the P_{Exp} (0–224 GPa) completed in the conventional DAC increases with increasing pressure, and the largest relative error reaches about 7%. Meanwhile, the difference between the P_{DIA} and the P_{Exp} (red stars in Figure 3c) at a higher compression range (160–280 GPa) performed in a tDAC decreases with increasing pressure, leading to a systematic error of larger than 10 GPa (in the green dashed circle) around 200 GPa. This uncertainty regarding the pressure is mainly a consequence of the markedly different degrees of non-hydrostatic effects on the Cu [50] and Au [49] pressure scales used in their respective DAC and tDAC experimental runs since, if only the X-ray diffraction peaks of the (111) lattice plane, least affected by uniaxial stress, of the Cu and Au were selected to determine the pressures, the mentioned systematic errors would disappear as indicated in Figure 3d. Comparatively, the calculated results by the DM agree well with the DAC measurements of Ref. [8] (black symbols in Figure 3c,d).

Almost at the same time as Storm et al. [8], Campbell et al. [9] reported three datasets on the compression of Bi in a DAC in a neon PTM, up to a maximum pressure of about 260 GPa. As shown by the red symbols in Figure 3e, the P_{DIA} agrees very well with the P_{Exp} below 75 GPa, over which the P_{DIA} deviates from the P_{Exp} gradually up to 5.8 GPa. Meanwhile, the DM manifests worse than the DIA, as indicated by the black symbols in Figure 3e. It should be pointed out that, in the first two experimental runs (run A and run B) of Ref. [9], the used Cu pressure scale [52] by Dewaele et al. was employed essentially to only 153 GPa, so the P_{Exp} values over 153 GPa in the run B measurements (16.8–184 GPa) are extrapolated results. Moreover, this Cu calibration determined by a ruby

scale [52] was indicated to underestimate the pressures [53,54]. To inspect these queries, we re-calibrate the pressures of experimental run A and run B of Ref. [9] with the latest Cu calibration proposed by Fratanduono et al. [50], which is also used as the pressure scale in the DAC measurements of Storm et al. [8]. As shown in Figure 3e,f, the pressures below 100 GPa estimated from the two different Cu pressure standards are nearly the same, while, above ~100 GPa, the recalibrated pressures are indeed larger than estimated by the scale of Dewaele et al. [52], and the maximum re-estimated pressure in experimental run B is 190.4 GPa (instead of 184 GPa). The pressures in run C experiment of Ref. [9] were determined by a neon EOS established by the authors based on the compression data measured in their run B experiment, in which neon and Cu were concurrently compressed, and the corresponding pressures were calibrated by the Cu EOS of Dewaele et al. [52]. So, the P_{Exp} over 153 GPa in the run C measurements (93.8–258.7 GPa) of Ref. [9] also included extended results that are actually unreliable. As the authors of Ref. [9] noted, if the pressures in their run C measurements were calibrated by the neon EOS promoted by Dewaele et al. [17], the evaluated pressures would be higher. As shown by the orange triangles in Figure 3f, since the neon EOS of Ref. [17] was proposed to 209 GPa, the recalibration with this neon scale for the pressures in the run C experiment of Ref. [9] is just 209 GPa. The difference between the P_{DIA} and the re-calibrated pressures increases with increasing pressure gradually up to 11.8 GPa, corresponding to a relative error $((P_{Exp} - P_{DIA})/P_{Exp})$ of 5.8%, which is two times larger than that displayed in Figure 3e. Distinctly, the accuracy of the measured EOS directly relies on the precision of the used pressure scale. Comparatively, the P_{DM} is much closer to the re-calibrated pressures in the pressure range of over 100 GPa, with the largest deviation of only ~6 GPa.

4. Discussion

As shown by the orange squares and stars in Figure 3f and the red squares in Figure 3d, under the same Cu pressure standard of Fratanduono et al. [50], the difference between the P_{DIA} and the P_{Exp} of Ref. [9] is smaller than that between the P_{DIA} and the P_{Exp} of Ref. [8] by only 2~3 GPa in a large pressure range (<200 GPa), revealing that the apparent discrepancy between the originally reported EOS of *bcc* Bi by Storm et al. [8] and Campbell et al. [9] is mainly caused by the system errors inherent in the different Cu calibrations promoted by Dewaele et al. [52] and Fratanduono et al. [50]. What is worth mentioning is that, in the low-pressure range (<75 GPa), the P_{DIA} nearly reproduces the result of Ref. [9], while it deviates from the measurement of Ref. [8] gradually with increasing pressure. Since a neon PTM was included in the experiment of Ref. [9] and not in Ref. [8], the hydrostatic condition in the former system should be better. This confirms the reliability of the DIA.

After re-calibrating the pressures in Ref. [10] with the latest Pt pressure scale proposed by Fratanduono et al. [49], the difference between the P_{DIA} and the re-evaluated pressures (brown symbols in Figure 3a) is nearly the same as that between the P_{DIA} and P_{Exp} of Ref. [8] (red squares in Figure 3d). So, if the latest Cu [50] and Pt [49] pressure scales both promoted by Fratanduono et al. are self-consistent, it can be concluded that the experimental EOSs of *bcc* Bi up to 200 GPa are nearly converged so far.

Whereas, as shown by the brown symbols in Figure 3a, red squares in Figure 3d, and orange symbols in Figure 3f, the calculated results by the DIA still display gradually increasing deviations from these experimental data, and the relative difference reaches about 7% at 200 GPa. It should be pointed out that both the Cu [50] and Pt [49] pressure scales by Fratanduono et al. were established via reducing the ramp-compressed stress-density data to the room-temperature isothermal data, so the accuracy of the Cu [50] and Pt [49] EOSs strongly depends on the reduction method. For the thermodynamic models used in Refs. [49,50], on the one hand, the thermal energies caused by the plastic work heating in the ramp compression were determined from the Debye integral, which is strongly related to the selection of the expression of the Grüneisen parameter. On the other hand, the Grüneisen parameters for the Cu [50] and Pt [49] were treated as simply volume-dependent, but they are actually both volume- and temperature-dependent. As a result,

these approximations may cause large deviations in the reduced isotherms of the Cu [50] and Pt [49] EOSs, particularly at high pressures. In fact, aside from the Debye integral and Grüneisen parameter, several other approximations were also used in Refs. [49,50]. As a reference, the uncertainty for the EOSs of Cu [50] and Pt [49] produced in the reduction process increases with increasing pressure and reaches about ±6 GPa at 200 GPa.

It is worth mentioning that a large uniaxial stress component was observed in the pressure marker Au used in the tDAC experiments of Ref. [8], so the corresponding measured pressures (red stars in Figure 3c,d) are seriously non-hydrostatic, which should be very different from the ones under hydrostatic conditions. As the authors of Ref. [8] estimated, the corrections for the pressures arising from the deviatoric stress on the Au pressure marker were as large as 39 GPa at the highest compression, while the largest deviatoric stress on the Cu was less than 2 GPa, so we think that the tDAC measurements of Ref. [8] could be optimized further using Cu as the pressure marker. As discussed in the last paragraph of Section 3, the pressure measurements over 153 GPa in Ref. [9] are extended results (Figure 3e), which are actually unreliable. So, the experimental EOS of *bcc* Bi over 200 GPa needs to be re-inspected in the future.

It should be pointed out that the background of the DM is the harmonic approximation, which works only at low temperatures. Furthermore, a previous theoretical study [55] showed that the precision of the harmonic approximation would become lower and lower with increasing atomic volume when the value is larger than 20 $Å^3$/atom. For the EOS of Bi at 300 K within 0~100 GPa, the harmonic approximation might not be a good approximation because the DM temperature is smaller than 300 K [45], and, as presented in Ref. [45], the atomic volume of Bi is larger than 20 $Å^3$/atom below 69 GPa. This may account for the worse agreement of the calculated results by the DM with the experimental measurements in the low-pressure range.

As indicated by Figure 3, our calculated results agree well with all the experimental measurements at low pressures, especially with Refs. [9,11], while showing increasing deviations in the high-pressure conditions. In addition to the discussions in the foregoing paragraphs, other possible causes for the differences between the calculated results and the experiments at high pressures should also be evaluated. As a matter of fact, the accuracy of the EOS calculated in the present work depends not only on the precision of the DIA but also on the calculated total energies ($U(\boldsymbol{q}^N)$) involved in the PF (Equation (1)). As for the precision of the DIA, it has been rigorously confirmed by the corresponding molecular dynamics simulations under the same interaction potentials as very accurate, with uncertainties of less than 1% for the pressure calculations in terms of the common condensed matter types [27]. What is more, the precision of the DIA indeed increases with decreasing atomic volume [27]. The accuracy of the total energies calculated in DFT mainly relies on the adopted pseudopotential and the exchange-correlation functional. Although the pseudopotential and GGA-PBE functional are commonly used in DFT calculations, we are unsure as to their validity at very high pressures up to 300 GPa. So, if the total energies under very high compressions calculated by DFT are accurate, the *bcc* Bi EOS provided in the present work would be reliable.

5. Conclusions

By directly solving the PF, we obtained the room-temperature isothermal EOS of *bcc* Bi. Compared with the DACs experiments, including the PTM, the deviations in the calculated results could be negligible below 75 GPa, while they gradually become larger at higher pressures and reach 12 GPa at 200 GPa, which may be caused by the inaccuracy of the pressure standard used in high-pressure conditions. Compared with the experiments with no PTM, the calculated pressures gradually depart from the measurements up to 16 GPa at 200 GPa, revealing the fact that the non-hydrostatic experiments cannot be described well by the theory of equilibrium statistics. In conclusion, the EOS provided in the present work is expected to be a reasonable standard for future static pressure measurements.

Author Contributions: Conceptualization, Y.-Y.T., B.-Y.N., H.-F.Z. and X.-J.N.; Data curation, Y.-Y.T., H.-F.Z. and X.-J.N.; Formal analysis, Y.-Y.T., H.-F.Z. and X.-J.N.; Methodology, B.-Y.N. and X.-J.N.; Project administration, Y.-Y.T., H.-F.Z. and X.-J.N.; Software, B.-Y.N.; Writing—original draft, Y.-Y.T.; Writing—review and editing, Y.-Y.T., H.-F.Z. and X.-J.N. All authors have read and agreed to the published version of the manuscript.

Funding: This research received no external funding.

Data Availability Statement: The original contributions presented in the study are included in the article, further inquiries can be directed to the corresponding authors.

Acknowledgments: We gratefully acknowledge Hongzhiwei Technology (Shanghai) Co., Ltd. for providing the computation resources.

Conflicts of Interest: Author Hui-Fen Zhang was employed by the company Hongzhiwei Technology (Shanghai) Co., Ltd. The remaining authors declare that the research was conducted in the absence of any commercial or financial relationships that could be construed as a potential conflict of interest.

References

1. Yaoita, K.; Tsuji, K.; Katayama, Y.; Imai, M.; Chen, J.-Q.; Kikegawa, T.; Shimomura, O. The structure of liquid bismuth under pressure. *J. Non-Cryst. Solids* **1992**, *150*, 25–28. [CrossRef]
2. McMahon, M.I.; Degtyareva, O.; Nelmes, R.J. Ba-IV-type incommensurate crystal structure in group-V metals. *Phys. Rev. Lett.* **2000**, *85*, 4896–4899. [CrossRef] [PubMed]
3. Duff, R.E.; Minshall, F.S. Investigation of a Shock-Induced Transition in Bismuth. *Phys. Rev.* **1957**, *108*, 1207–1212. [CrossRef]
4. Aoki, K.; Fujiwara, S.; Kusakabe, M. Stability of the *bcc* structure of bismuth at high pressure. *J. Phys. Soc. Jpn.* **1982**, *51*, 3826–3830. [CrossRef]
5. Degtyareva, O.; McMahon, M.I.; Nelmes, R.J. High-pressure structural studies of group-15 elements. *High Press. Res.* **2004**, *24*, 319–356. [CrossRef]
6. Ono, S. High-pressure phase transition of bismuth. *High Press. Res.* **2018**, *38*, 414–421. [CrossRef]
7. Husband, R.J.; O'Bannon, E.F.; Liermann, H.-P.; Lipp, M.J.; Méndez, A.S.J.; Konôpková, Z.; McBride, E.E.; Evans, W.J.; Jenei, Z. Compression-rate dependence of pressure-induced phase transitions in Bi. *Sci. Rep.* **2021**, *11*, 14859. [CrossRef] [PubMed]
8. Storm, C.V.; McHardy, J.D.; Duff, M.J.; MacLeod, S.G.; O'Bannon, E.F., III; McMahon, M.I. The stress state in bismuth to 298 GPa and its use as a pressure transmitting medium and pressure marker at multi-megabar pressures. *J. Appl. Phys.* **2023**, *133*, 245904. [CrossRef]
9. Campbell, D.J.; Sneed, D.T.; O'Bannon, E.F.; Söderlind, P.; Jenei, Z. Refined room-temperature equation of state of Bi up to 260 GPa. *Phys. Rev. B* **2023**, *107*, 224104. [CrossRef]
10. Akahama, Y.; Kawamura, H.; Singh, A.K. Equation of state of bismuth to 222 GPa and comparison of gold and platinum pressure scales to 145 GPa. *J. Appl. Phys.* **2002**, *92*, 5892–5897. [CrossRef]
11. Liu, L.; Song, H.X.; Geng, H.Y.; Bi, Y.; Xu, J.-a.; Li, X.; Li, Y.; Liu, J. Compressive behaviors of bcc bismuth up to 55 GPa. *Phys. Status. Solidi.* **2013**, *250*, 1398–1403. [CrossRef]
12. Katahara, K.W.; Manghnani, M.H.; Fisher, E.S. Pressure derivatives of the elastic moduli of niobium and tantalum. *J. Appl. Phys.* **1976**, *47*, 434–439. [CrossRef]
13. Holzapfel, W.B.; Hartwig, M.; Sievers, W. Equations of state for Cu, Ag, and Au for wide ranges in temperature and pressure up to 500 GPa and above. *J. Phys. Chem. Ref. Data* **2001**, *30*, 515–529. [CrossRef]
14. Qi, X.; Cai, N.; Wang, S.; Li, B. Thermoelastic properties of tungsten at simultaneous high pressure and temperature. *J. Appl. Phys.* **2020**, *128*, 105105. [CrossRef]
15. Jamieson, J.; Fritz, J.N.; Manghanani, M.H. Pressure measurement at high temperature in x-ray diffraction studies: Gold as a primary standard, in High-Pressure Research in Geophysics. *Adv. Earth Planet. Sci.* **1980**, *12*, 27.
16. Holmes, N.C.; Moriarty, J.A.; Gathers, G.R.; Nellis, W.J. The equation of state of platinum to 660 GPa (6.6 Mbar). *J. Appl. Phys.* **1989**, *66*, 2962–2967. [CrossRef]
17. Dewaele, A.; Datchi, F.; Loubeyre, P.; Mezouar, M. High pressure-high temperature equations of state of neon and diamond. *Phys. Rev. B* **2008**, *77*, 094106. [CrossRef]
18. Vinet, P.; Ferrante, J.; Rose, J.H.; Smith, J.R. Compressibility of solids. *J. Geophys. Res. Solid Earth* **1987**, *92*, 9319–9325. [CrossRef]
19. Vinet, P.; Ferrante, J.; Smith, J.R.; Rose, J.H. A universal equation of state for solids. *J. Phys. C Solid State Phys.* **1986**, *19*, L467. [CrossRef]
20. Birch, F. Finite strain isotherm and velocities for single-crystal and polycrystalline NaCl at high pressures and 300 K. *J. Geophys. Res. Solid Earth* **1978**, *83*, 1257–1268. [CrossRef]
21. Murnaghan, F.D. Finite deformations of an elastic solid. *Am. J. Math.* **1937**, *59*, 235–260. [CrossRef]
22. Holzapfel, W.B. Equations of state for solids under strong compression. *High Press. Res.* **1998**, *16*, 81–126. [CrossRef]
23. Holzapfel, W.B. Physics of solids under strong compression. *Rep. Prog. Phys.* **1996**, *59*, 29. [CrossRef]

24. Gaurav, S.; Sharma, B.S.; Sharma, S.B.; Upadhyaya, S.C. Analysis of equations of state for solids under high compressions. *Physica B* **2002**, *322*, 328–339. [CrossRef]
25. Burakovsky, L.; Burakovsky, N.; Cawkwell, M.J.; Preston, D.L.; Errandonea, D.; Simak, S.I. Ab initio phase diagram of iridium. *Phys. Rev. B* **2016**, *94*, 094112. [CrossRef]
26. Gutiérrez, G.; Menéndez-Proupin, E.; Singh, A.K. Elastic properties of the *bcc* structure of bismuth at high pressure. *J. Appl. Phys.* **2006**, *99*, 103504. [CrossRef]
27. Ning, B.-Y.; Gong, L.-C.; Weng, T.-C.; Ning, X.-J. Efficient approaches to solutions of partition function for condensed matters. *J. Phys. Condens. Matter* **2021**, *33*, 115901. [CrossRef] [PubMed]
28. Han, J.; Shi, L.-Q.; Wang, N.; Zhang, H.-F.; Peng, S.-M. Equation of state of Iridium: From insight of ensemble theory. *J. Phys. Condens. Matter* **2022**, *34*, 465702. [CrossRef]
29. Gong, L.-C.; Ning, B.-Y.; Weng, T.-C.; Ning, X.-J. Comparison of Two Efficient Methods for Calculating Partition Functions. *Entropy* **2019**, *21*, 1050. [CrossRef]
30. Liu, Y.-P.; Ning, B.-Y.; Gong, L.-C.; Weng, T.-C.; Ning, X.-J. A New Model to Predict Optimum Conditions for Growth of 2D Materials on a Substrate. *Nanomaterials* **2019**, *9*, 978. [CrossRef]
31. Ning, B.-Y.; Ning, X.-J. Pressure-induced structural phase transition of vanadium: A revisit from the perspective of ensemble theory. *J. Phys. Condens. Matter* **2022**, *34*, 425404. [CrossRef] [PubMed]
32. Ning, B.-Y. Pressure-induced structural phase transitions of zirconium: An ab initio study based on statistical ensemble theory. *J. Phys. Condens. Matter* **2022**, *34*, 505402. [CrossRef] [PubMed]
33. Ning, B.-Y.; Zhang, L.-Y. An ab initio study of structural phase transitions of crystalline aluminium under ultrahigh pressures based on ensemble theory. *Comput. Mater. Sci.* **2023**, *218*, 111960. [CrossRef]
34. Tian, Y.-Y.; Ning, B.-Y.; Zhang, H.-F.; Ning, X.-J. Equation of state for tungsten obtained by direct solving the partition function. *J. Appl. Phys.* **2024**, *135*, 015102. [CrossRef]
35. Dierckx, P. An algorithm for smoothing, differentiation and integration of experimental data using spline functions. *J. Comput. Appl. Math.* **1975**, *1*, 165–184. [CrossRef]
36. Kresse, G.; Furthmüller, J. Efficiency of ab-initio total energy calculations for metals and semiconductors using a plane-wave basis set. *Comput. Mater.* **1996**, *6*, 15–50. [CrossRef]
37. Kresse, G.; Furthmüller, J. Efficient iterative schemes for ab initio total-energy calculations using a plane-wave basis set. *Phys. Rev. B* **1996**, *54*, 11169–11186. [CrossRef] [PubMed]
38. Blöchl, P.E. Projector augmented-wave method. *Phys. Rev. B* **1994**, *50*, 17953–17979. [CrossRef]
39. Kresse, G.; Joubert, D. From ultrasoft pseudopotentials to the projector augmented-wave method. *Phys. Rev. B* **1999**, *59*, 1758–1775. [CrossRef]
40. Perdew, J.P.; Burke, K.; Ernzerhof, M. Generalized Gradient Approximation Made Simple. *Phys. Rev. Lett.* **1996**, *77*, 3865–3868. [CrossRef]
41. Chen, H.-Y.; Xiang, S.-K.; Yan, X.-Z.; Zheng, L.-R.; Zhang, Y.; Liu, S.-G.; Bi, Y. Phase transition of solid bismuth under high pressure. *Chin. Phys. B* **2016**, *25*, 108103. [CrossRef]
42. Fan, X.; Xiang, S.; Cai, L. Temperature dependence of bismuth structures under high pressure. *Chin. Phys. B* **2022**, *31*, 056101. [CrossRef]
43. Munoz, F.; Vergniory, M.G.; Rauch, T.; Henk, J.; Chulkov, E.V.; Mertig, I.; Botti, S.; Marques, M.A.L.; Romero, A.H. Topological Crystalline Insulator in a New Bi Semiconducting Phase. *Sci. Rep.* **2016**, *6*, 21790. [CrossRef] [PubMed]
44. Freitas, R.R.Q.; Rivelino, R.; de Brito Mota, F.; de Castilho, C.M.C.; Kakanakova-Georgieva, A.; Gueorguiev, G.K. Topological Insulating Phases in Two-Dimensional Bismuth-Containing Single Layers Preserved by Hydrogenation. *J. Phys. Chem. C* **2015**, *119*, 23599–23606. [CrossRef]
45. Mukherjee, D.; Sahoo, B.D.; Joshi, K.D.; Gupta, S.C. On equation of state, elastic, and lattice dynamic stability of *bcc* bismuth under high pressure: Ab-initio calculations. *J. Appl. Phys.* **2014**, *115*, 053702. [CrossRef]
46. Xiang, S.; Xi, F.; Bi, Y.; Xu, J.a.; Geng, H.; Cai, L.; Jing, F.; Liu, J. Ab initio thermodynamics beyond the quasiharmonic approximation: W as a prototype. *Phys. Rev. B* **2010**, *81*, 014301. [CrossRef]
47. Wang, Y.; Chen, D.; Zhang, X. Calculated Equation of State of Al, Cu, Ta, Mo, and W to 1000 GPa. *Phys. Rev. Lett.* **2000**, *84*, 3220–3223. [CrossRef] [PubMed]
48. Burakovsky, L.; Burakovsky, N.; Preston, D.; Simak, S. Systematics of the Third Row Transition Metal Melting: The HCP Metals Rhenium and Osmium. *Crystals* **2018**, *8*, 243. [CrossRef]
49. Fratanduono, D.E.; Millot, M.; Braun, D.G.; Ali, S.J.; Fernandez-Pañella, A.; Seagle, C.T.; Davis, J.-P.; Brown, J.L.; Akahama, Y.; Kraus, R.G.; et al. Establishing gold and platinum standards to 1 terapascal using shockless compression. *Science* **2021**, *372*, 1063–1068. [CrossRef]
50. Fratanduono, D.E.; Smith, R.F.; Ali, S.J.; Braun, D.G.; Fernandez-Pañella, A.; Zhang, S.; Kraus, R.G.; Coppari, F.; McNaney, J.M.; Marshall, M.C.; et al. Probing the solid phase of noble metal copper at terapascal conditions. *Phys. Rev. Lett.* **2020**, *124*, 015701. [CrossRef]
51. Jin, K.; Wu, Q.; Geng, H.; Li, X.; Cai, L.; Zhou, X. Pressure-volume-temperature equations of state of Au and Pt up to 300 GPa and 3000 K: Internally consistent pressure scales. *High Press. Res.* **2011**, *31*, 560–580. [CrossRef]
52. Dewaele, A.; Loubeyre, P.; Mezouar, M. Equations of state of six metals above 94 GPa. *Phys. Rev. B* **2004**, *70*, 094112. [CrossRef]

53. Dorogokupets, P.I.; Oganov, A.R. Ruby, metals, and MgO as alternative pressure scales: A semiempirical description of shock-wave, ultrasonic, X-ray, and thermochemical data at high temperatures and pressures. *Phys. Rev. B* **2007**, *75*, 024115. [CrossRef]
54. Sokolova, T.S.; Dorogokupets, P.I.; Litasov, K.D. Self-consistent pressure scales based on the equations of state for ruby, diamond, MgO, B2-NaCl, as well as Au, Pt, and other metals to 4 Mbar and 3000 K. *Russ. Geol. Geophys.* **2013**, *54*, 181–199. [CrossRef]
55. Gong, L.-C.; Ning, B.-Y.; Ming, C.; Weng, T.-C.; Ning, X.-J. How accurate for phonon models to predict the thermodynamics properties of crystals. *J. Phys. Condens. Matter* **2021**, *33*, 085901. [CrossRef]